Eur. Phys. J. C 46, 465–473 (2006)
Digital Object Identifier (DOI) 10.1140/epjc/s2006-02523-9

THE EUROPEAN PHYSICAL JOURNAL C

Probing the color glass condensate in an electron-ion collider

M.S. Kugeratski[1,a], V.P. Gonçalves[2], F.S. Navarra[1]

[1] Instituto de Física, Universidade de São Paulo, C.P. 66318, 05315-970 São Paulo, SP, Brazil
[2] High and Medium Energy Group (GAME), Instituto de Física e Matemática, Universidade Federal de Pelotas, Caixa Postal 354, CEP 96010-900, Pelotas, RS, Brazil

Received: 15 November 2005 / Revised version: 17 February 2006 /
Published online: 30 March 2006 –

Abstract. Perturbative quantum chromodynamics (pQCD) predicts that the small-x gluons in a hadron wavefunction should form a color glass condensate (CGC), characterized by a saturation scale $Q_s(x, A)$, which is energy and atomic number dependent. In this paper, we study the predictions of CGC physics for electron-ion collisions at high energies. We consider that the nucleus at high energies acts as an amplifier of the physics of high parton densities and estimate the nuclear structure function $F_2^A(x, Q^2)$, as well as the longitudinal and charm contributions, using a generalization for nuclear targets of the Iancu–Itakura–Munier model that describes the ep HERA data quite well. Moreover, we investigate the behavior of the logarithmic slopes of the total and longitudinal structure functions in the kinematical region of the future electron-ion collider eRHIC.

In the high energy limit, perturbative quantum chromodynamics (pQCD) predicts that the small-x gluons in a hadron wavefunction should form a color glass condensate (CGC), which is described by an infinite hierarchy of coupled evolution equations for the correlators of Wilson lines [1–4]. In the absence of correlations, the first equation in the Balitsky–JIMWLK hierarchy decouples and is then equivalent to the equation derived independently by Kovchegov within the dipole formalism [5]. The Balitsky–Kovchegov (BK) equation describes the energy evolution of the dipole-target scattering amplitude $\mathcal{N}(x, \mathbf{r})$. Although a complete analytical solution is still lacking, its main properties are known (for recent reviews see, e.g. [6–9]): (a) for the interaction of a small dipole ($\mathbf{r} \ll 1/Q_{\rm s}$), $\mathcal{N}(\mathbf{r}) \approx \mathbf{r}^2$, implying that this system is weakly interacting; and (b) for a large dipole ($\mathbf{r} \gg 1/Q_{\rm s}$), the system is strongly absorbed and, therefore, $\mathcal{N}(\mathbf{r}) \approx 1$. This property is associated to the large density of saturated gluons in the hadron wave function. Furthermore, several groups have studied the numerical solution of the BK equation [10–12] and have confirmed many of the theoretical predictions. In particular, the studies presented in [11, 12] have demonstrated that the BK solution for fixed constant coupling preserves the atomic number dependence of the saturation scale present in the initial condition, while for running α_s this dependence is reduced with increasing rapidity, as predicted by Mueller in [13].

The search for signatures of parton saturation effects has been an active subject of research in the last years (for recent reviews see, e.g. [6, 9, 14]). On the one hand, it has been observed that the HERA data at small x and low Q^2 can be successfully described with the help of saturation models [15–19], with the experimental results for the total cross section [20] and inclusive charm production [21] presenting the property of geometric scaling. On the other hand, the recently observed [22] suppression of high p_T hadron yields at forward rapidities in dAu collisions at RHIC has the behavior anticipated on the basis of CGC ideas [23–26]. All these results provide strong evidence for the CGC physics at HERA and RHIC. However, more definite conclusions are not possible due to the small value of the saturation scale in the kinematical range of HERA and due to the complexity present in the description of dAu collisions, where we need to consider the substructure of the projectile and target, as well as the fragmentation of the produced partons. As a direct consequence, other models are able to describe the same set of data (see, e.g. [27, 28]). In order to discriminate between these different models and test the CGC physics, it would be very important to consider an alternative search. To this purpose, the future electron-nucleus colliders are ideal, because they can probably determine whether parton distributions saturate and constrain the behavior of the nuclear gluon distribution. This expectation can easily be understood if we assume the empirical parameterization $Q_{\rm s}^2 = A^{\frac{1}{3}} \times Q_0^2 \, \left(\frac{x_0}{x}\right)^{\lambda}$, with the parameters $Q_0^2 = 1.0\,\mathrm{GeV}^2$, $x_0 = 0.267 \times 10^{-4}$ and $\lambda = 0.253$ as in [18]. We can observe that, while in the proton case we need very small values of x to obtain large values of $Q_{\rm s}^2$, in the nuclear case a similar value can be obtained for values of x approximately two orders of magnitude greater. Consequently, nuclei are an efficient amplifier of parton densities. The parton density that would be accessed in an electron-ion collider would be

[a] e-mail: barros@ufpel.edu.br

equivalent to that obtained in an electron-proton collider at energies that are at least one order of magnitude higher than at HERA [29].

Recently, at RHIC an electron-ion collider has been proposed in order to explore the relevant physics of polarized and unpolarized electron-nucleus collisions [30]. In particular, this collider will explore the high density regime of QCD, even though its $x-Q^2$ range will be somewhat less extensive than that achieved at HERA. For instance, with energies $\sqrt{s}=60$–$100\,\mathrm{GeV}$, one will access $x\approx 10^{-4}-10^{-3}$ for $Q^2\approx 1$–$10\,\mathrm{GeV}^2$, respectively. However, the saturation scale will be approximately $4.0\,\mathrm{GeV}^2$ at small x, low Q^2 and $A=197$. Furthermore, as pointed out in [30], in principle all the inclusive and semi-inclusive observables that were studied at HERA can be studied at eRHIC. This collider is expected to have statistics high enough to allow for the determination of the logarithmic slopes with respect to x and Q^2 of the total and longitudinal structure functions. In particular, the longitudinal structure function is expected to be measured for the first time in the kinematical regime of small x, since the electron-ion collider will be able to vary the energies of both the electron and ion beams. It will be possible to check predictions made by CGC inspired models (which have been extensively tested at HERA) for the behavior of these observables.

In this paper, we study the behavior of the total, longitudinal and charm structure functions in the kinematical region that will be probed in electron-ion collisions at RHIC considering a generalization for nuclear targets of the saturation model proposed by Iancu, Itakura and Munier (IIM model). Moreover, we estimate the logarithmic slopes of the total and longitudinal structure functions at different values of the atomic number. We hope that our results will contribute to the planning of future eA experiments (for previous studies, see [31–47]).

We start from the space-time picture of the electron-proton/nuclei processes [48]. In the rest frame of the target, the QCD description of DIS at small x can be interpreted as a two-step process. The virtual photon (emitted by the incident electron) splits into a $q\bar{q}$ dipole, which subsequently interacts with the target. In terms of virtual photon-target cross sections $\sigma_{T,L}$ for the transversely and longitudinally polarized photons, the F_2 structure function is given by [48]

$$F_2(x,Q^2)=\frac{Q^2}{4\pi^2\alpha_{em}}(\sigma_T+\sigma_L) \tag{1}$$

and

$$\sigma_{T,L}=\int d^2\mathbf{r}\,dz\,|\Psi_{T,L}(\mathbf{r},z,Q^2)|^2\;\sigma_{\mathrm{dip}}(x,\mathbf{r})\;, \tag{2}$$

where $\Psi_{T,L}$ is the light-cone wave function of the virtual photon and σ_{dip} is the dipole cross section describing the interaction of the $q\bar{q}$ dipole with the target. In equation (2) $\mathbf{r}$ is the transverse separation of the $q\bar{q}$ pair and z is the photon momentum fraction carried by the quark (for details see, e.g. [49]).

The dipole hadron cross section σ_{dip} contains all information about the target and the strong interaction physics. In the CGC formalism [2–4], σ_{dip} can be computed in the eikonal approximation and is given by:

$$\sigma_{dip}(x,\mathbf{r})=2\int d^2\mathbf{b}\,\mathcal{N}(x,\mathbf{r},\mathbf{b})\;, \tag{3}$$

where $\mathcal{N}$ is the dipole-target forward scattering amplitude for a given impact parameter $\mathbf{b}$ that encodes all the information about the hadronic scattering, and thus about the non-linear and quantum effects in the hadron wave function. The function $\mathcal{N}$ can be obtained by solving the BK (JIMWLK) evolution equation in the rapidity $Y\equiv\ln(1/x)$. It is useful to assume that the impact parameter dependence of $\mathcal{N}$ can be factorized as $\mathcal{N}(x,\mathbf{r},\mathbf{b})=\mathcal{N}(x,\mathbf{r})S(\mathbf{b})$, so that $\sigma_{dip}(x,\mathbf{r})=\sigma_0\,\mathcal{N}(x,\mathbf{r})$, with σ_0 being a free parameter related to the non-perturbative QCD physics. Several models for the dipole cross section have been used in the literature in order to fit the HERA data [15–19]. Here we will consider only the model proposed in [18], where the dipole-target forward scattering amplitude was parameterized as follows:

$$\mathcal{N}(x,\mathbf{r})=\begin{cases}\mathcal{N}_0\,\left(\frac{\mathbf{r}\,Q_s}{2}\right)^{2\left(\gamma_s+\frac{\ln(2/\mathbf{r}Q_s)}{\kappa\,\lambda\,Y}\right)}\;, & \text{for } \mathbf{r}Q_s(x)\leq 2\;,\\ 1-\exp^{-a\,\ln^2(b\,\mathbf{r}\,Q_s)}\;, & \text{for } \mathbf{r}Q_s(x)>2\;,\end{cases} \tag{4}$$

where the expression for $\mathbf{r}Q_s(x)>2$ (saturation region) has the correct functional form, as obtained either by solving the BK equation [2, 5], or from the CGC theory [6]. Hereafter, we label the above model as IIM. The coefficients a and b are determined from the continuity conditions of the dipole cross section at $\mathbf{r}Q_s(x)=2$. The coefficients $\gamma_s=0.63$ and $\kappa=9.9$ are fixed from their LO BFKL values and $\sigma_0=2\pi R_p^2$, where R_p is the proton radius. In further calculations we shall use the parameters $R_p=0.641$ fm, $\lambda=0.253$, $x_0=0.267\times10^{-4}$ and $\mathcal{N}_0=0.7$, which give the best fit result. Recently, this model was also used in phenomenological studies of vector meson production [50] and diffractive processes [51] at HERA, as well as for the description of the longitudinal structure function [52].

Some comments related to the IIM model are in order here. Firstly, it is important to emphasize that this model is constructed by smoothly interpolating between two limiting cases that are analytically under control, but have leading order accuracy. The first line of (4) is obtained from the solution of the BFKL equation via a saddle point approximation, valid for very high energies and very small dipole sizes. The thus obtained solution is then further expanded under the assumption that the dipole sizes are close to the saturation radius. Secondly, it is valid only in a limited range of virtualities, such that the DGLAP evolution can be disregarded and the scaling solution of the BFKL equation can be used. Moreover, the free parameters in the IIM model have been determined without including the charm, i.e. considering only three active flavors. Consequently, our predictions for the nuclear charm structure function should be considered as a rough estimate of this observable. However, we believe that our main conclusions related to $F_2^{c,A}$ are not modified if a new fit including the charm is performed.

We generalize the IIM model for nuclear collisions assuming the following basic transformations: $\sigma_0 \to \sigma_0^A = A^{\frac{2}{3}} \times \sigma_0$ and $Q_s^2(x) \to Q_{s,A}^2 = A^{\frac{1}{3}} \times Q_s^2(x)$. Moreover, in order to estimate the contribution of the saturation physics in the following we present a comparison between the full IIM model and the predictions from linear physics, obtained by extrapolating the expression of $\mathcal{N}(x, \mathbf{r})$, valid for $\mathbf{r}Q_s(x) \leq 2$, for the entire kinematical range. In our calculations, the impact parameter dependence of the scattering amplitude, which is mainly associated to non-perturbative physics, is disregarded. Basically, following [18], we shall treat the nucleus as a homogeneous disk of radius R_A. Consequently, with this model we cannot discuss the expansion of the transverse size of the target with increasing energy. Furthermore, we assume that the $A^{\frac{1}{3}}$-dependence of the nuclear saturation scale is preserved by the evolution. This assumption is valid in the fixed coupling case, where the A scaling of the initial condition survives without changing the evolution. On the other hand, for a running coupling, the $A^{\frac{1}{3}}$ scaling holds only in a limited kinematical range, with the nuclear dependence becoming weaker at larger energies [13]. In this case, we can expect that the $A^{\frac{1}{3}}$-dependence of the nuclear saturation scale will be slightly modified at eRHIC. It is important to emphasize that more sophisticated generalizations to the nuclear case can be used (see, e.g. [17, 39, 42, 47]). Consequently, this work should be considered as an exploratory study whose main goal is to present a semiquantitative estimate of the CGC effects in the future eA collider. In a full calculation we must use the solution of the BK equation, obtained without neglecting the impact parameter dependence, as well as an initial condition constrained by current experimental lepton-nucleus data.

Before presenting our results for the total, longitudinal and charm structure function, we can investigate the mean dipole size dominating each of these cross sections. We define the photon-nucleus overlap function, normalized by the atomic number A, as follows:

$$H_i\left(\mathbf{r}, x, Q^2\right) = \frac{2\pi \mathrm{r}}{A} \times \int dz \left|\Psi_i(z,\, \mathbf{r}, m_f, Q^2)\right|^2 \sigma_{dip}(x, \mathbf{r}, A)\,, \tag{5}$$

where $i = T,\, L$ characterizes transverse and longitudinal photons. In particular, we also calculate the overlap function associated to the total structure function, $H_2\left(\mathbf{r}, x, Q^2\right) \equiv H_T\left(\mathbf{r}, x, Q^2\right) + H_L\left(\mathbf{r}, x, Q^2\right)$, and the overlap function associated to the charm structure function, $H_c\left(\mathbf{r}, x, Q^2\right)$, which is calculated using $m_f = m_c = 1.5\,\mathrm{GeV}$. In Figs. 1, 2 and 3 we show the distinct overlap functions (normalized by A) as functions of the dipole size for different values of x, A and Q^2. The first aspect that should be emphasized is that although the overlap functions have been normalized by A, they are strongly A-dependent. This behavior is expected when we consider the full prediction of the IIM model. However, our results demonstrate that this dependence is also present when we calculate the overlap functions using the linear approximation. It is associated to the $[Q_{s,A}^2(x)]^{\gamma_{\mathrm{eff}}}$-dependence of the dipole scattering amplitude, where $\gamma_{\mathrm{eff}} = \gamma_s + \frac{\ln(2/\mathbf{r}Q_s)}{\kappa\,\lambda\,Y}$ in the IIM model. For $\gamma_{\mathrm{eff}} = 1$, we will have an $A^{\frac{1}{3}}$-dependence for $\mathcal{N}$, which combined with the $A^{\frac{2}{3}}$-dependence of σ_0 implies a linear A-dependence for the dipole cross section in the linear regime. If normalized by A, we will obtain an A-independent overlap function in the linear regime. However, since $\gamma_{\mathrm{eff}} < 1$ in the IIM model, the overlap function (and the corresponding observables) has an $A^{\frac{\gamma_{\mathrm{eff}}-1}{3}}$-dependence, i.e. it decreases with increasing atomic number. This behavior is observed in the figures. In Fig. 1 we estimate the overlap functions

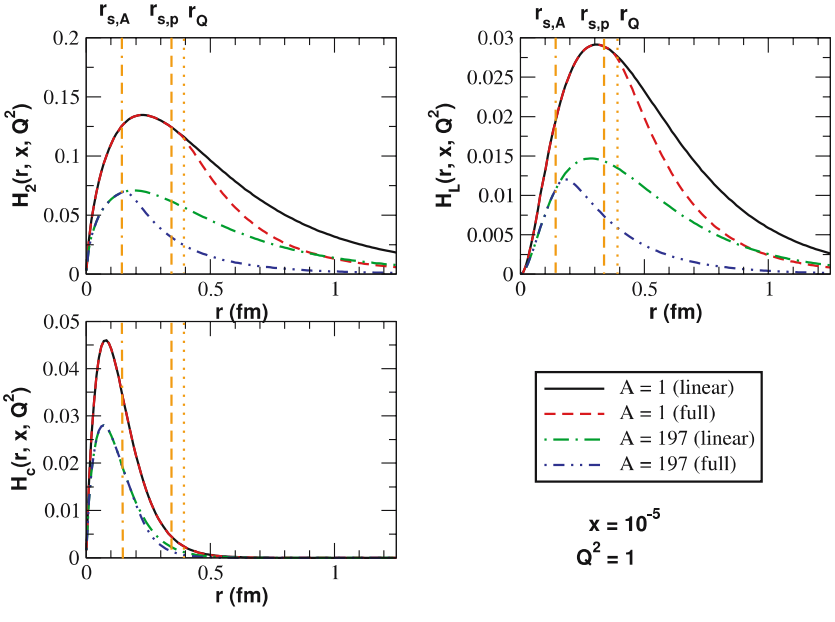

Fig. 1. The $\mathbf{r}$-dependence of the photon-nucleus overlap functions, normalized by A, for different values of the atomic number ($x = 10^{-5}$ and $Q^2 = 1\,\mathrm{GeV}^2$)

for fixed x ($= 10^{-5}$) and $Q^2 (= 1\,\mathrm{GeV}^2)$, and two values of the atomic number. In order to illustrate our results, we define the quantities $\mathbf{r}_{s,A} \equiv 2/Q_{s,A}$, $\mathbf{r}_{s,p} \equiv 2/Q_{s,p}$ and $\mathbf{r}_Q \equiv 2/Q$, which are directly associated to the nuclear, proton saturation scale and photon virtuality, respectively. The value of these quantities is indicated in Figs. 1 and 2 by vertical lines. We have $\mathbf{r}_{s,A} < \mathbf{r}_{s,p} < \mathbf{r}_Q$ at $Q^2 = 1\,\mathrm{GeV}^2$, while $\mathbf{r}_Q < \mathbf{r}_{s,A} < \mathbf{r}_{s,p}$ at $Q^2 = 10\,\mathrm{GeV}^2$. We can see that the charm overlap function is peaked at approximately $\mathbf{r} \approx 0.07$ fm, which agrees with the theoretical expectation that the $c\bar{c}$ pair has a typical transverse size $\approx 1/\mu$, where $\mu \equiv \sqrt{Q^2 + 4m_c^2}$ (see a similar discussion in [40]). Therefore, the main contribution to the cross section comes from the small dipole sizes, i.e. from the region where the saturation effects are small (linear regime). This expectation is confirmed by the behavior of the overlap function H_c, which is the same in the linear and full predictions for fixed A. Therefore, we should expect that the modifications in the charm structure function due to saturation effects will be small. This is expected, since the typical scale for charm production, μ^2, is larger than the saturation scale $Q^2_{s,A}$ in all kinematical ranges of eRHIC, i.e. at this collider it is expected that the linear regime dominates the heavy quark production (see the discussion in [21]). On the other hand, for light quark production, a broader $\mathbf{r}$ distribution is obtained, peaked at large values of the pair separation, $\mathbf{r} \approx \mathbf{r}_{s,p}\,(\mathbf{r}_{s,A})$ at $A = 1$ (197), implying that saturation effects contribute significantly in this case. This same feature is observed in the behavior of the overlap functions H_2 and H_L presented in Fig. 1. In this case, we can see that the saturation effects suppress the contribution of large dipole size, as expected theoretically. Moreover, these effects become more important for smaller values of x and larger A. We can observe that the area under the curve is significantly reduced by the saturation effects, which implies that the associated observable will be strongly modified by these effects. In Fig. 2, we present the behavior of H_2 and H_L for $Q^2 = 10\,\mathrm{GeV}^2$. In this case, we observe that the distributions peak at smaller values of the dipole size, $\mathbf{r} \approx \mathbf{r}_Q$, with the contribution of large dipole size being reduced. This implies that for $A = 1$, the full and linear predictions are identical. For large nuclei ($A = 197$) saturation effects still contribute, which implies a reduction of the area under the curve and a modification of the associated observable. The charm overlap function (not shown) has identical behavior for the linear and full predictions, and the two values of the atomic number. We can conclude that the saturation effects are strongly reduced for large values of Q^2.

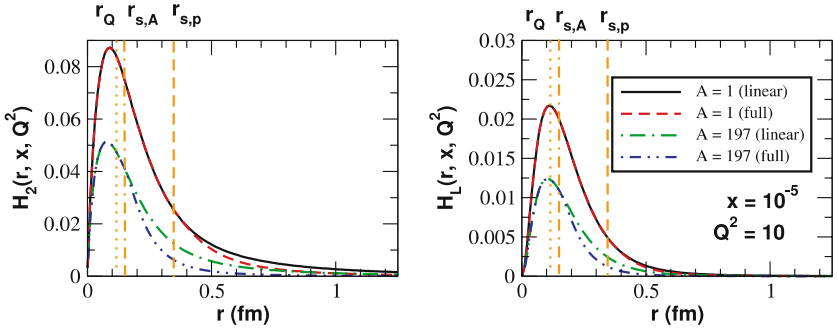

Fig. 2. The $\mathbf{r}$-dependence of the photon-nucleus overlap functions, normalized by A, for different values of the atomic number ($x = 10^{-5}$ and $Q^2 = 10\,\mathrm{GeV}^2$)

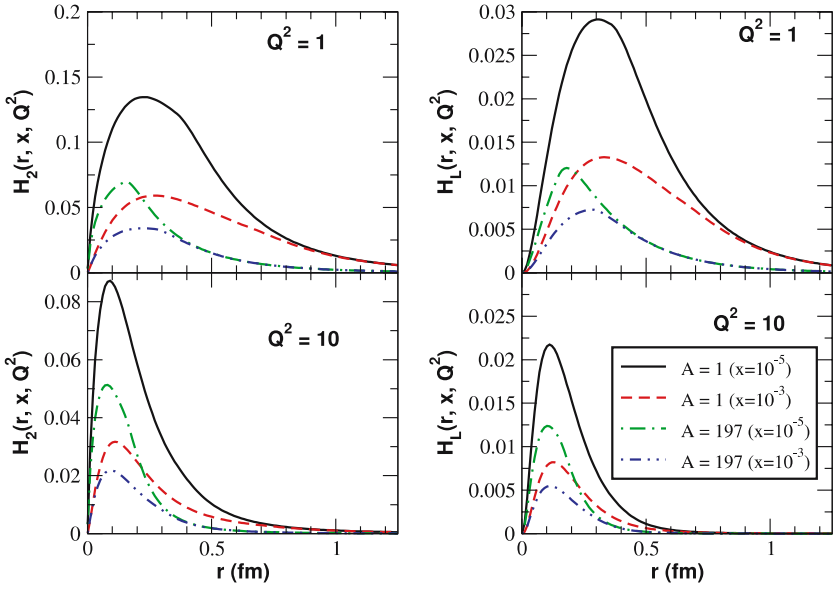

Fig. 3. The $\mathbf{r}$-dependence of the photon-nucleus overlap functions, normalized by A, for different values of the atomic number, x and Q^2

In Fig. 3, we present the H_2 and H_L overlap functions for two values of x and Q^2. In this figure, we show only the full predictions. As discussed before: (a) by increasing Q^2 the distributions peak at small values of the dipole size; and (b) the area under the curve is reduced by increasing the atomic number. The main aspect of this figure is that it allows us to analyze the x-dependence of the overlap function. We observe that by decreasing x, the overlap function grows, with the growth being smaller for large nuclei. Consequently, we expect that the associated observables increase at small x, with a smaller slope for $A = 197$. These expectations are confirmed in Fig. 4, where we present the x-dependence of the total, longitudinal and charm structure functions. We can see that the full and linear predictions for the charm structure function are identical, having the A-dependence characteristic of the IIM model. On the other hand, the behavior of F_2^A and F_L^A is strongly modified by saturation physics, with the effect decreasing for larger Q^2. In order to obtain a more precise estimate of the modification in the observables, in Fig. 5 we present the ratios R_{F_2} and R_{F_L} between the full and linear predictions for F_2 and F_L, respectively. We consider three typical values of the atomic number. As expected, the contribution of the saturation physics increases at large nuclei and smaller values of x. In particular, for values of x around 10^{-5}, we predict a reduction of about 50% in the total and longitudinal structure functions. In Fig. 6, we present the behavior of the ratio between the nuclear and proton structure functions, $R(x, Q^2) \equiv F_2^A(x, Q^2)/F_2^p(x, Q^2)$, as a function of x and Q^2. For comparison, the predictions of the EKS parameterization [53], which is a global fit of the nuclear experimental data using the DGLAP equation, is

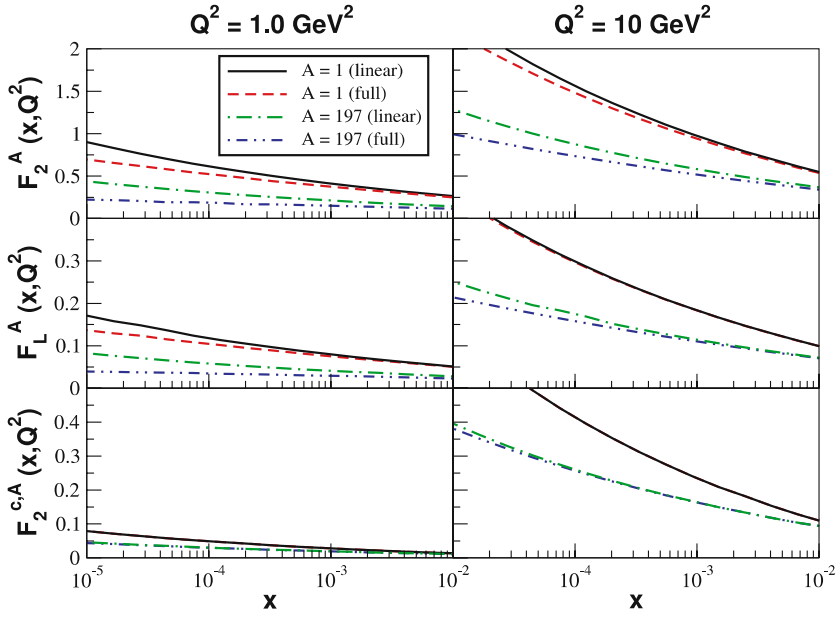

Fig. 4. Nuclear structure functions as a function of x for different values of A and Q^2

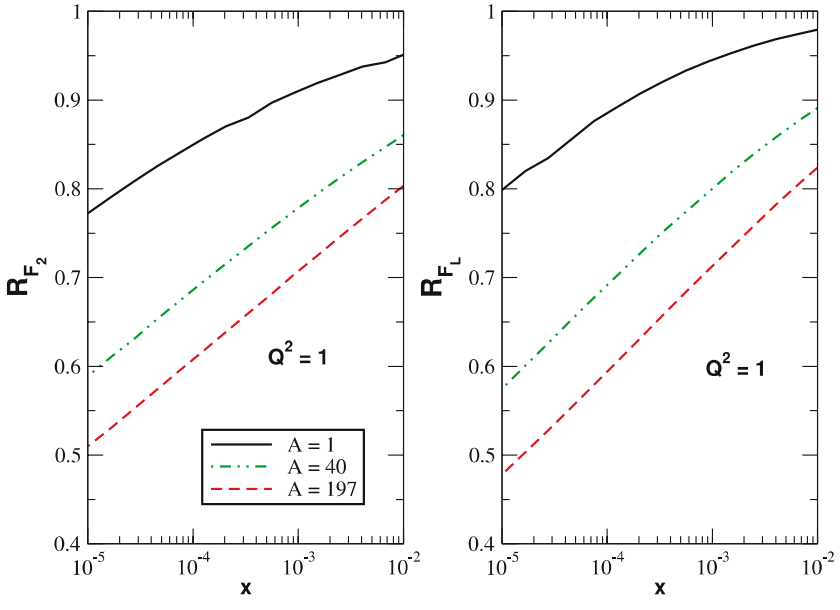

Fig. 5. Ratio between the full and linear predictions for the different nuclear structure functions

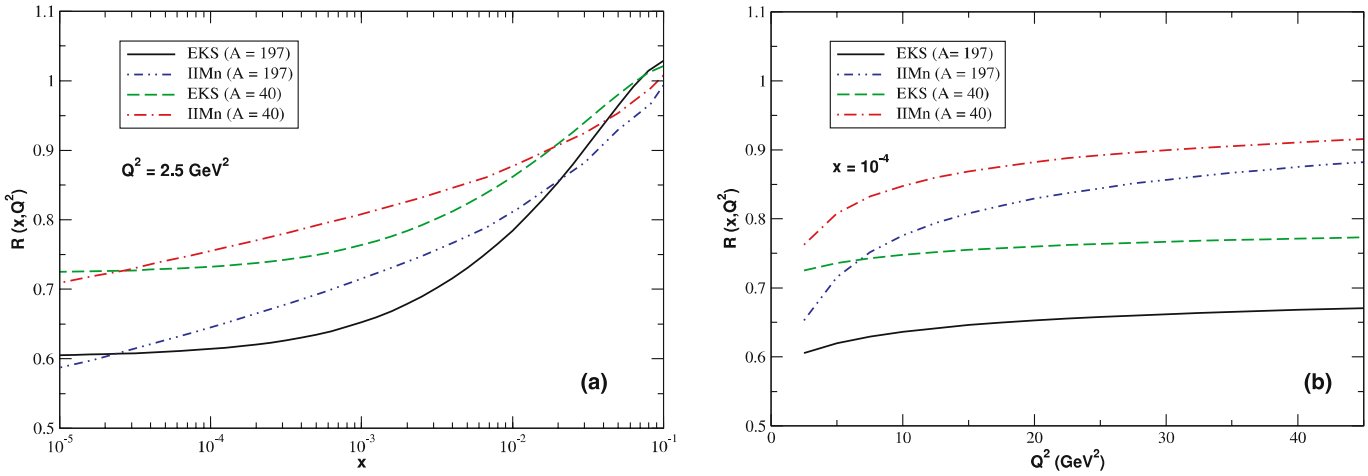

Fig. 6. Ratio $R(x,Q^2) \equiv F_2^A(x,Q^2)/F_2^p(x,Q^2)$ as a function of **a** x and **b** Q^2. The predictions of the EKS parameterization are shown for comparison

also presented. In particular, in Fig. 6 (a) we show the behavior of this ratio as a function of x at $Q^2 = 2.5\,\mathrm{GeV}^2$, assuming two different values of A: 197 and 40. We can see that, similarly to EKS parameterization, the ratio obtained using the IIM model generalized for nuclear targets (IIMn) decreases when A increases. The main difference between the predictions is the behavior of the ratio R at small x. While the EKS parameterization predicts that the ratio is constant in this limit, IIMn predicts that the ratio still decreases at smaller values of x. In Fig. 6 (b), we present the Q^2-dependence of the ratio at $x = 10^{-4}$. We find that while this behavior in the EKS parameterization is directly associated to the DGLAP evolution, in the IIMn prediction it is associated to the saturation and geometric scaling regime. We see that the predictions differ significantly at small values of Q^2, where saturation physics dominates.

Other observables of interest to study the CGC physics are the logarithmic slopes of F_2 and F_L with respect to x and Q^2. They are mainly motivated by the strict relation between the gluon distribution and the scaling violations of the total structure function at leading order in the DGLAP formalism [54]. In the dipole formalism, the scaling violations are directly related to the dipole cross section (see, e.g. [56])

$$\frac{dF_2(x,Q^2)}{d\log Q^2} \approx Q^2 \times \sigma_{dip}\left(x, \mathbf{r}^2 = \frac{4}{Q^2}\right) \ . \qquad (6)$$

Therefore, this observable can be useful for addressing the boundary between the linear and saturation regimes [34]. This expectation is easily understood. As this observable is strongly dependent on the dipole cross section and it presents a distinct behavior for $Q^2 > Q_s^2$ and $Q^2 < Q_s^2$, its experimental analysis would allow us to test the x-dependence and A-dependence of the saturation scale. On the other hand, the logarithmic derivative of F_2 with respect to x is directly related with the power of growth of this structure function at small x. Basically, if we parameterize the total structure function using $F_2^A\,(x,Q^2) = x^{-\lambda(x,Q^2,A)}$, we obtain

$$\frac{d\log F_2^A\,(x,Q^2)}{d\log 1/x} = \lambda\left(x,Q^2,A\right) \ , \qquad (7)$$

i.e. this logarithmic slope is directly related to the effective pomeron intercept (for a similar analysis in ep collisions see, e.g. [55]). In Fig. 7 (a), we present the Q^2-dependence of the effective intercept for $x = 10^{-3}$ and different values of the atomic number. For comparison, the prediction of the GBW model generalized for nuclear targets is also presented. For small values of Q^2, both models predict a similar dependence for λ. The main difference occurs in the region of large values of Q^2, where their predictions are not expected to be valid. However, an A-dependence for λ is observed, λ being smaller for large nuclei. This behavior can be understood considering the prediction of the IIM model for F_2^A in the region $\mathbf{r}Q_s(x) \leq 2$ (linear regime). In this case, we obtain that the effective power $\lambda(x,Q^2,A)$ is proportional to $\frac{\gamma_{\mathrm{eff}}-1}{3}\ln A/\ln(1/x)$ (plus positive A-independent terms), which is negative, since $\gamma_{\mathrm{eff}} < 1$, and grows in the modulus with A. Moreover, this agrees with our previous results, where we found that the growth of the nuclear structure function at small x decreases at larger A. In Fig. 7 (b), the x-dependence of the intercept for $Q^2 = 1\,\mathrm{GeV}^2$ is shown. In this case, we only consider the IIM model and show its linear and full predictions. We can see that the linear predictions for λ are similar. On the other hand, the saturation effects imply that λ decreases at small x, its reduction being stronger for $A = 197$.

In Fig. 8, we present the x-dependence of the logarithmic derivatives of F_2 and F_L with respect to Q^2. These derivatives, as well as λ, have been evaluated numerically using the DFRIDR routine [57], which is based on Richardson's deferred approach to the limit. We can see that both derivatives have similar behavior, with the linear and full predictions being identical for large x. For the F_2 slope and $A = 1$, the difference between the linear and full predictions starts at $x \approx 10^{-4}$, increasing at smaller values of x. On the other hand, at $A = 197$ both predictions differ at values of

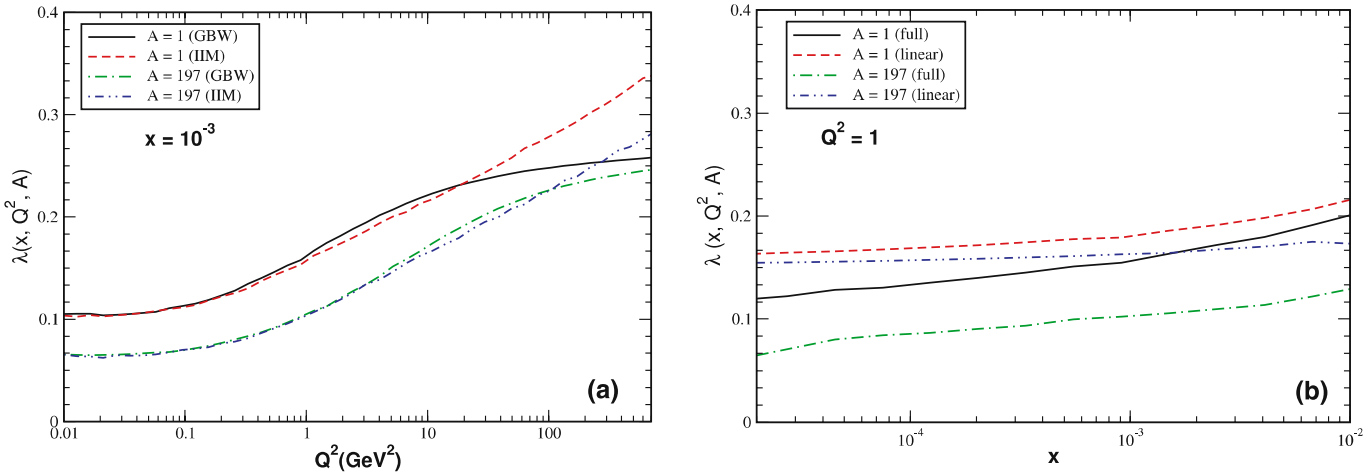

Fig. 7. Effective intercept as a function of: **a** Q^2 and **b** x

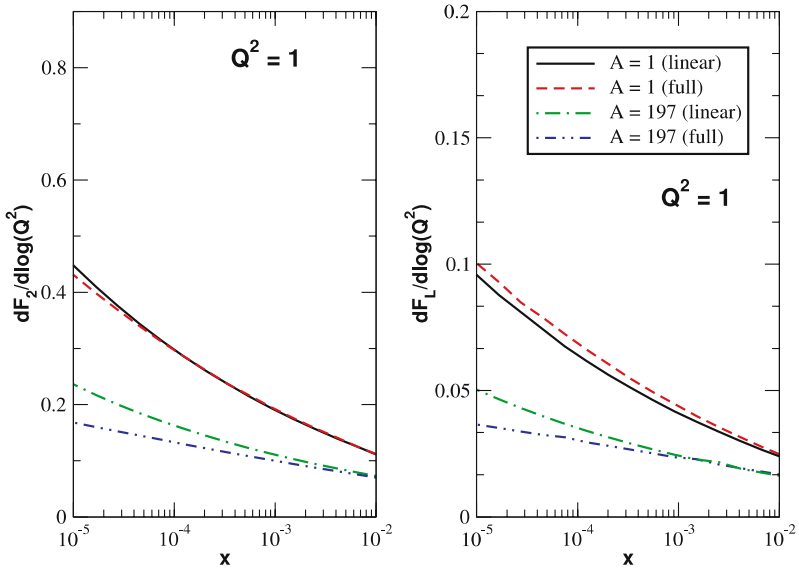

Fig. 8. Logarithmic slope with respect to Q^2 of the total and longitudinal structure functions

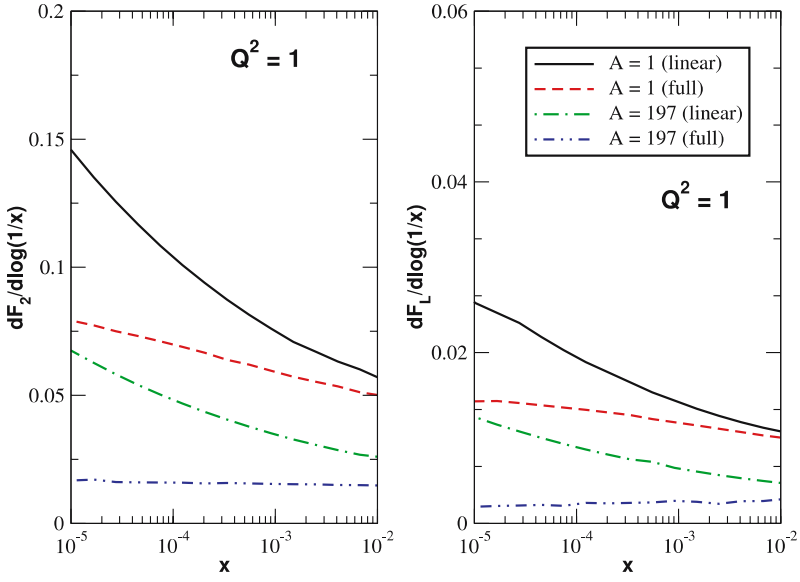

Fig. 9. Logarithmic slope with respect to x of the total and longitudinal structure functions

x smaller than $\approx 10^{-2}$, with a large difference between the predictions at small x. For the F_L slope and $A = 197$, we have a similar behavior, but with the difference between the predictions starting at $x \approx 10^{-3}$. At $A = 1$ we can see that the full prediction is larger than the linear one for the x range of the figure. We have found that at smaller values of x, the linear prediction becomes larger than the full one. Finally, in Fig. 9 we present the x-dependence of the logarithmic derivatives of F_2 and F_L with respect to x. We can see that while the linear predictions grow at small x, the full predictions present a smaller slope. In particular, at $A = 197$ these observables are almost x-independent when we consider the saturation effects.

As a summary, in this paper we have studied the predictions of CGC physics for electron-ion collisions at high energies, using a generalization for nuclear targets of the Iancu–Itakura–Munier model, which describes the *ep* HERA quite well. We have estimated the nuclear structure function $F_2^A(x, Q^2)$, as well as the longitudinal and charm contributions. Moreover, we have investigated the behavior of the logarithmic slopes of the total and longitudinal structure functions in the kinematical region of the future electron-ion collider eRHIC. Our results indicate that the experimental analysis of these observables in the future electron-ion collider could discriminate between linear and saturation physics, as well as constrain the behavior of the saturation scale. Our analysis was restricted to inclusive observables. However, CGC physics also strongly modifies the behavior of exclusive observables, as verified, for instance, in diffractive processes at HERA. Studies of diffractive interactions in eA interactions are still scarce. Some examples are those performed in [40, 46], where the diffractive photoproduction of heavy quark and vector mesons in eA collisions were studied. In a forthcoming publication [58], we calculate the nuclear diffractive structure function, finding that the analysis of this observable can be useful to constrain CGC physics.

Acknowledgements. This work was partially financed by the Brazilian funding agencies CNPq, FAPESP and FAPERGS.

References

1. L. McLerran, R. Venugopalan, Phys. Rev. D **49**, 2233 (1994); ibid. **49**, 3352 (1994); ibid. **50**, 2225 (1994)
2. I.I. Balitsky, Nucl. Phys. B **463**, 99 (1996); Phys. Rev. Lett. **81**, 2024 (1998); Phys. Rev. D **60**, 014020 (1999); Phys. Lett. B **518**, 235 (2001); I.I. Balitsky, A.V. Belitsky, Nucl. Phys. B **629**, 290 (2002)
3. E. Iancu, A. Leonidov, L. McLerran, Nucl. Phys. A **692**, 583 (2001); E. Ferreiro, E. Iancu, A. Leonidov, L. McLerran, Nucl. Phys. A **701**, 489 (2002)
4. J. Jalilian-Marian, A. Kovner, L. McLerran, H. Weigert, Phys. Rev. D **55**, 5414 (1997); J. Jalilian-Marian, A. Kovner, H. Weigert, Phys. Rev. D **59**, 014014 (1999); ibid. **59**, 014015 (1999), ibid. **59** 034007 (1999); A. Kovner, J. Guilherme Milhano, H. Weigert, Phys. Rev. D **62**, 114005 (2000); H. Weigert, Nucl. Phys. A **703**, 823 (2002)
5. Y.V. Kovchegov, Phys. Rev. D **60**, 034008 (1999); ibid. **61** 074018 (2000)
6. E. Iancu, R. Venugopalan, arXiv:hep-ph/0303204
7. A.M. Stasto, Acta Phys. Polon. B **35**, 3069 (2004)
8. H. Weigert, Prog. Part. Nucl. Phys. **55**, 461 (2005)
9. J. Jalilian-Marian, Y.V. Kovchegov, Prog. Part. Nucl. Phys. **56**, 104 (2006)
10. M.A. Braun, Eur. Phys. J. C **16**, 337 (2000); N. Armesto, M.A. Braun, Eur. Phys. J. C **20**, 517 (2001); M.A. Kimber, J. Kwiecinski, A.D. Martin, Phys. Lett. B **508**, 58 (2001); E. Levin, M. Lublinsky, Nucl. Phys. A **696**, 833 (2001); M. Lublinsky, Eur. Phys. J. C **21**, 513 (2001); M. Lublinsky, E. Gotsman, E. Levin, U. Maor, Nucl. Phys. A **696**, 851 (2001); K. Golec-Biernat, L. Motyka, A.M. Stasto, Phys. Rev. D **65**, 074037 (2002); K. Golec-Biernat, A.M. Stasto, Nucl. Phys. B **668**, 345 (2003); E. Gotsman, M. Kozlov, E. Levin, U. Maor, E. Naftali, Nucl. Phys. A **742**, 55 (2004); K. Kutak, A.M. Stasto, Eur. Phys. J. C **41**, 343 (2005); G. Chachamis, M. Lublinsky, A. Sabio Vera, Nucl. Phys. A **748**, 649 (2005); T. Ikeda, L. McLerran, Nucl. Phys. A **756**, 385 (2005); C. Marquet, G. Soyez, Nucl. Phys. A **760**, 208 (2005); R. Enberg, K. Golec-Biernat, S. Munier, Phys. Rev. D **72**, 074021 (2005)
11. K. Rummukainen, H. Weigert, Nucl. Phys. A **739**, 183 (2004)
12. J.L. Albacete, N. Armesto, J.G. Milhano, C.A. Salgado, U.A. Wiedemann, Phys. Rev. D **71**, 014003 (2005)
13. A.H. Mueller, Nucl. Phys. A **724**, 223 (2003)
14. V.P. Goncalves, M.V.T. Machado, Mod. Phys. Lett. **19**, 2525 (2004)
15. K. Golec-Biernat, M. Wüsthoff, Phys. Rev. D **59**, 014017 (1999), ibid. D **60**, 114023 (1999)
16. J. Bartels, K. Golec-Biernat, H. Kowalski, Phys. Rev. D **66**, 014001 (2002)
17. H. Kowalski, D. Teaney, Phys. Rev. D **68**, 114005 (2003)
18. E. Iancu, K. Itakura, S. Munier, Phys. Lett. B **590**, 199 (2004)
19. J.R. Forshaw, G. Shaw, JHEP **0412**, 052 (2004)
20. A.M. Staśto, K. Golec-Biernat, J. Kwieciński, Phys. Rev. Lett. **86**, 596 (2001)
21. V.P. Goncalves, M.V.T. Machado, Phys. Rev. Lett. **91**, 202002 (2003)
22. BRAHMS Collaboration, I. Arsene et al., Phys. Rev. Lett. **91**, 072305 (2003); Phys. Rev. Lett. **93**, 242303 (2004); Phys. Rev. Lett. **94**, 032301 (2005); arXiv:nucl-ex/0410020
23. R. Baier, A. Kovner, U.A. Wiedemann, Phys. Rev. D **68**, 054009 (2003); J. Jalilian-Marian, Y. Nara, R. Venugopalan, Phys. Lett. B **577**, 54 (2003); D. Kharzeev, Y.V. Kovchegov, K. Tuchin, Phys. Rev. D **68**, 094013 (2003); J.L. Albacete, N. Armesto, A. Kovner, C.A. Salgado, U.A. Wiedemann, Phys. Rev. Lett. **92**, 082001 (2004); E. Iancu, K. Itakura, D.N. Triantafyllopoulos, Nucl. Phys. A **742**, 182 (2004)
24. J. Jalilian-Marian, Nucl. Phys. A **748**, 664 (2005)
25. D. Kharzeev, Y.V. Kovchegov, K. Tuchin, Phys. Lett. B **599**, 23 (2004)
26. A. Dumitru, A. Hayashigaki, J. Jalilian-Marian, Nucl. Phys. A **765**, 464 (2006); arXiv:hep-ph/0512129
27. J.R. Forshaw, G. Kerley, G. Shaw, Phys. Rev. D **60**, 074012 (1999); J.R. Forshaw, G.R. Kerley, G. Shaw, Nucl. Phys. A **675**, 80C (2000)
28. R.C. Hwa, C.B. Yang, R.J. Fries, Phys. Rev. C **71**, 024902 (2005); J. w. Qiu, I. Vitev, Phys. Lett. B **632**, 507

(2006); B.Z. Kopeliovich, J. Nemchik, I.K. Potashnikova, M.B. Johnson, I. Schmidt, arXiv:hep-ph/0501260
29. R. Venugopalan, AIP Conf. Proc. **588**, 121 (2001) [arXiv:hep-ph/0102087]
30. A. Deshpande, R. Milner, R. Venugopalan, W. Vogelsang, Ann. Rev. Nucl. Part. Sci. **55**, 165 (2005)
31. A.L. Ayala Filho, M.B. Gay Ducati, E.M. Levin, Nucl. Phys. B **493**, 305 (1997)
32. M.B. Gay Ducati, V.P. Goncalves, Phys. Lett. B **466**, 375 (1999)
33. M.B. Gay Ducati, V.P. Goncalves, Phys. Rev. C **60**, 058 201 (1999)
34. V.P. Goncalves, Phys. Lett. B **495**, 303 (2000)
35. E. Gotsman, E. Levin, U. Maor, L.D. McLerran, K. Tuchin, Nucl. Phys. A **683**, 383 (2001)
36. A.L. Ayala Filho, V.P. Goncalves, Eur. Phys. J. C **20**, 343 (2001)
37. N. Armesto, M.A. Braun, Eur. Phys. J. C **22**, 351 (2001)
38. E. Levin, M. Lublinsky, Nucl. Phys. A **696**, 833 (2001)
39. N. Armesto, Eur. Phys. J. C **26**, 35 (2002)
40. V.P. Goncalves, M.V.T. Machado, Eur. Phys. J. C **30**, 387 (2003)
41. N. Armesto, A. Capella, A.B. Kaidalov, J. Lopez-Albacete, C.A. Salgado, Eur. Phys. J. C **29**, 531 (2003)
42. J. Bartels, E. Gotsman, E. Levin, M. Lublinsky, U. Maor, Phys. Rev. D **68**, 054008 (2003)
43. A. Freund, K. Rummukainen, H. Weigert, A. Schafer, Phys. Rev. Lett. **90**, 222 002 (2003)
44. E. Gotsman, E. Levin, M. Lublinsky, U. Maor, E. Naftali, Acta Phys. Polon. B **34**, 3255 (2003)
45. V.P. Goncalves, M.V.T. Machado, Eur. Phys. J. C **32**, 501 (2004)
46. V.P. Goncalves, M.V.T. Machado, Eur. Phys. J. C **38**, 319 (2004)
47. N. Armesto, C.A. Salgado, U.A. Wiedemann, Phys. Rev. Lett. **94**, 022 002 (2005)
48. N.N. Nikolaev, B.G. Zakharov, Z. Phys. C **49**, 607 (1991); Z. Phys. C **53**, 331 (1992); A.H. Mueller, Nucl. Phys. B **415**, 373 (1994); A.H. Mueller, B. Patel, Nucl. Phys. B **425**, 471 (1994)
49. V. Barone, E. Predazzi, High-Energy Particle Diffraction (Springer, Berlin Heidelberg, New York, 2002)
50. J.R. Forshaw, R. Sandapen, G. Shaw, Phys. Rev. D **69**, 094 013 (2004)
51. J.R. Forshaw, R. Sandapen, G. Shaw, Phys. Lett. B **594**, 283 (2004)
52. V.P. Goncalves, M.V.T. Machado, Eur. Phys. J. C **37**, 299 (2004)
53. K.J. Eskola, V.J. Kolhinen, C.A. Salgado, Eur. Phys. J. C **9**, 61 (1999)
54. K. Prytz, Phys. Lett. B **311**, 286 (1993); A.J. Askew, K. Golec-Biernat, J. Kwiecinski, A.D. Martin, P.J. Sutton, Phys. Lett. B **325**, 212 (1994); R.K. Ellis, Z. Kunszt, E.M. Levin, Nucl. Phys. B **420**, 517 (1994); Erratum-ibid. B **433**, 498 (1995); M.B. Gay Ducati, V.P. Goncalves, Phys. Lett. B **390**, 401 (1997)
55. M.B. Gay Ducati, K. Kontros, A. Lengyel, M.V.T. Machado, Phys. Lett. B **533**, 43 (2002)
56. A. L. . Ayala, M.B. Gay Ducati, E.M. Levin, Phys. Lett. B **388**, 188 (1996)
57. W.H. Press et al., Cambridge University Press, New York (1992)
58. M.S. Kugeratski, V.P. Goncalves, F.S. Navarra, Eur. Phys. J. C (in press) [arXiv:hep-ph/0511224]